Borotellurite bio-silica glasses doped by erbium nanoparticles: structural and thermal properties

Abdulkarim Muhammad Hamza[1,2,3], Umar Sa'ad Aliyu[1,3], Halimah Mohamed Kamari[1], Ibrahim Gana Geidam[1,4], Raouf El-Mallawany[5]*, Nazrin Nazrin[1], Muhammad Nasirudeen Baba [3]

Abstract

$[\{[(TeO_2)_{0.8} (B_2O_3)_{0.2}]_{0.8} (SiO_2)_{0.2}\}_{0.99} (Ag_2O)_{0.01}]_{1-y}$ - $(Er_2O_3\ NPs)_y$, and y=0.01,0.02,0.03,0.04 and 0.05 mole% were fabricated by the melt quenching technique. X-ray diffraction (XRD) was used to verify and confirm the glasses' non-crystallinity. X-ray fluorescence (XRF) proved the achievement of silicate of 98.6% quality from rice husk. Fourier transform infrared d (FTIR) results exposed the basic structural units such as TeO_4, TeO_3, BO_4, BO_3, Si-O-Si, and O-Si-O within the network. The concentration of Er_2O_3 nanoparticles' effects on the thermal properties of ErDBST glasses was duly discussed. From the profiling of the differential scanning calorimetry (DSC), the glass crystallization temperature T_c, and transition temperature T_g are estimated. Also, the thermal stability factor, defined as $T_s = T_c - T_g$, was higher than 100 ^oC. From room temperature above the T_g for all the sample glasses, specific heat capacity C_q (≥ 1.4J/gK^{-1}) was obtained. The results showed that the glass thermal stability and the transition temperature increase with the addition of Er_2O_3 nanoparticles (NPs). These suggest that an ErDBST glass exhibit good thermal stability and consequently is a suitable candidate for fiber drawing.

Keywords
Structural properties, Thermal properties, Glasses, Erbium nanoparticles .

[1] *Department of Physics, Faculty of Science, Universiti Putra Malaysia, 43400 UPM Serdang, Selangor, Malaysia.*
[2] *National Agency for Science and Engineering Infrastructure, Idu, Abuja, Nigeria.*
[3] *Department of Physics, Faculty of Sciences, Federal University of Lafia, Nasarawa State, Nigeria.*
[4] *Department of Physics, Faculty of Science, Yobe State University Damaturu, Nigeria.*
[5] *Department of Physics, Faculty of Science, Menoufia University, Egypt.*
***Corresponding author**: raoufelmallawany@yahoo.com

1. Introduction

The rare-earth ions (RE^{3+}) applications now cover almost all necessary fields of technology. For a material scientist to find out the applications for these specific ions, the requirements are studying the properties (structural and thermal) of feasible materials like glasses and their relationship with macroscopic properties. However, to understand the required glass properties suitable for optical devices, detailed theoretical knowledge on the optical improvement mechanism resulting from the embedded NPs doped into the host glass is very important [1–3]. The use of silicon oxide (SiO$_2$) as substrates for radiation shielding, optical fibers, electronic displays, and medical and dental implants is recommended to achieve mechanically strong glass [4]. Another thing of immense interest due to their high refractive indices both linear and non-linear, good chemical durability, good mechanical strength, and excellent transmission in the infrared wavelength and visible regions is the applications of tellurite glasses [5–10]. In recent times, glasses with modified optical properties for many technical and scientific applications have been made with two or more glass formers. The clean borate glasses have

a high melting point, low refractive index, and high phonon energies, approximately 1300–1500 cm^{-1} [11–15]. They are good at designing novel optical materials due to their easy fabrication, cost-effectiveness, and good solubility in RE ion on large-scale shaping. Though, the unsuitability for efficient IR to visible up-convertor of the borate glasses results from their high vibrational energy [16]. Lakshminaraya et al. [17] investigated the thermal and structural properties of zinc molybdenum borotellurite glasses with different network modifier ions. Besides the above, tellurite glasses have an interesting physical properties [18–21]. Furthermore, studies on thermal properties as specific heat capacity from DSC analysis have never been disclosed. Therefore, a glass system with five different chemical compositions in this study was fabricated, characterized, and investigated in the aspect of thermal properties as above mentioned.

The objectives of this article were to investigate both structural and thermal properties of the prepared glass series after to extraction of silicate from the rice husk, also to explore the possibility of the use of the studied glasses in fiber drawing. Parameters such as T_c, T_g, T_s =T_c-T_g, and C_q of the glasses were also investigated and studied.

Figure 1. XRD spectra of ErDBST glass doped with erbium oxide nanoparticles.

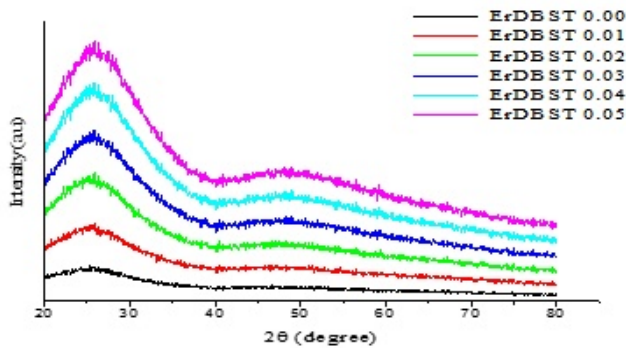**Figure 2.** FTIR spectra of ErDBST glasses doped with erbium oxide nanoparticles.

2. Experimental procedure

Fabrication of glasses with chemical compositions of $[\{[(TeO_2)_{0.8}(B_2O_3)_{0.2}]_{0.8}(SiO_2)_{0.2}\}_{0.99}(Ag_2O)_{0.01}]_{1-y}(Er_2O_3\ NPs)_y$, represented by ErDBST was achieved using melt quenching technique. Reagent grade oxides (99.99% purity, Alfar Aesar) and (98.6 % SiO_2 from rice husk) were used as preparatory materials. The oxides mixed were melted in alumina crucibles at a temperature of 1100 ^{o}C for 3 hours. The melted glass oxides were transferred into a stainless mold. The glass (as-prepared sample) was annealed at 400 ^{o}C (for one hour 30 min) instantly after the quench and gradually cooled to room temperature. The process of annealing is to lessen the internal mechanical stress and obtain a mechanically stable glass. The 400 ^{o}C chosen for annealing was since other glasses with similar compositions were treated at the same temperature and is enough to decrease/eliminate the internal tensions (Jlassi et al., 2011). The glasses obtained were crushed to meet the requirements for structural and DSC analysis. The glasses' thermal properties were studied using DSC in the range of room temperature to 1600 ^{o}C under air condition, at a heating rate of 10.00 ^{o}C/min via thermogravimetric analyzer (TGA/DSC) machine Metler Toledo brand (model TGA/DSC 1HT). The FTIR measurements of glass samples were carried out in the range of 200 to 4000 cm^{-1} by using Perkin Elmer FTIR 1660. Using X-ray fluorescence (XRF), the chemical quantitative analysis of the rice husk powder was achieved.

3. Results and discussion

The major elements present in rice husk ash that is essential in forming glass were analyzed using XRF, as shown in Table 1. Based on the XRF results, the primary component with 98.6 % is silica amid other compounds present, including SO3, CaO, K2O, Fe2O3, Ho2O3, MnO, CuO, and ZnO that can also serve as modifiers within the glass network. As typical requirements for silica from quartz, a larger percentage of iron of about 0.20% is accepted [22]. Though, Silica extracted from rice husk ash was purer compared to commercial silica, shown to be 98% pure [22], which is less than the extracted one. Also, the percentage of iron oxide (0.059%) in commercial silica is
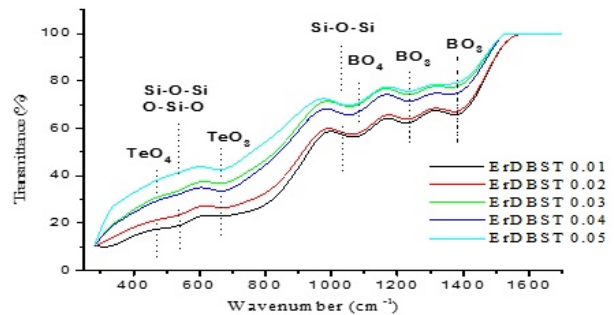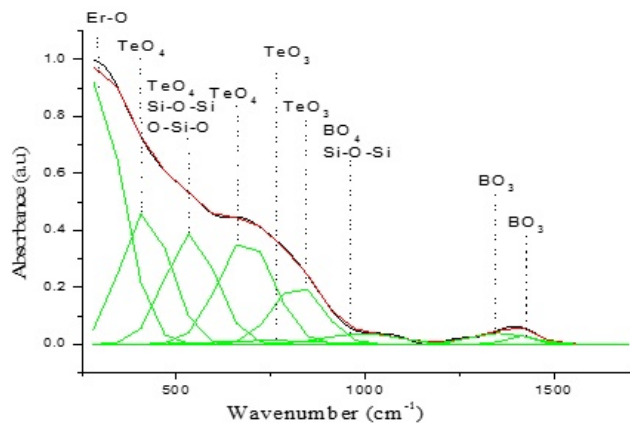

Figure 3. Deconvolution of the FTIR spectra spectrum for 0.03 ErDBST glass using a Gaussian-type function.

lower than that in the extracted silica from rice husk (0.091%). Moreover, the iron oxide appearance in the silica source only affects the resultant color of the glass. The iron oxide has a higher percentage which makes the colorless glass dark slightly. Consequently, its presence in the rice husk source should be controlled in the making of glass.

3.1 Spectra of XRD and FTIR

Firstly, for all the samples, the XRD analysis was conducted to pattern the nature (non-crystalline) of the glasses, and the result is given in Figure 1. It is observed that the results failed to indicate any sharp peaks but showed a broad hump between $20 - 35^o$ therefore, affirming the samples' amorphous nature [23]. Figure 2 shows the FTIR spectra for all studied glasses. The analysis is used to study the different functional group that exists in the glass network. The peak appears weak at 670 cm^{-1} due to the characteristics of pure TeO_2 glass and assigned to vibrations of TeO_3 and TeO_4 structural units [24]. FTIR spectra of the two glass series are in the range of $518 - 547\ cm^{-1}$, $667 - 674\ cm^{-1}$, $800 - 1200\ cm^{-1}$, and $1397 - 1440\ cm^{-1}$ which make up the four absorption bands. However, the deconvolution revealed some vibrations at $218 - 292\ cm^{-1}$ and $367 - 493\ cm^{-1}$. The absorption peaks of keen interest occur around $250 - 300\ cm^{-1}$, which
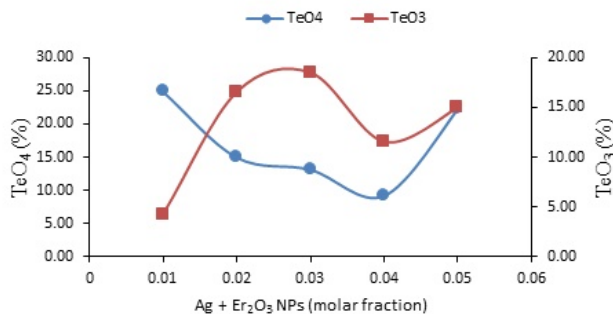
Figure 4. Band area of TeO_4 and TeO_3 structural units for borotellurite silicate glass doped with erbium oxide nanoparticles with silver oxide.
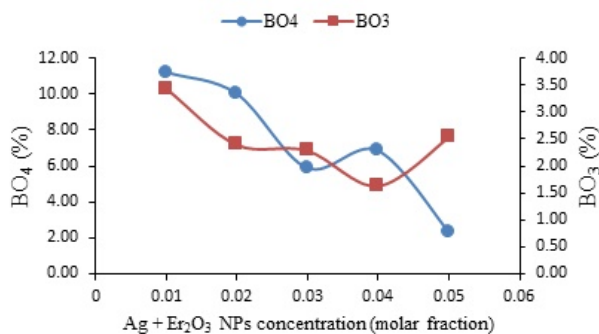

Figure 5. Band area of BO_4 and BO_3 structural units for borotellurite silicate glass doped with erbium oxide nanoparticles with silver oxide.

can be attributed to both $Er-O$ and TeO_3 tp bonds in the network of the glass system [5]. The presence of bands around $518-547$ cm^{-1} is assigned to the stretching vibrations of the TeO_4 trigonal bipyramid, which suggests the possibility of coordination transformation of TeO_4 to TeO_3 via TeO_{3+1} unit [25]. The vibration bands around $667-674$ cm^{-1} are attributed to the vibration of Te–O bonds in [TeO_4] tbp groups with bridging oxygen [26]. The band around $684-820$ cm^{-1} is attributed to the vibration of Te–O- in [TeO_3] tp groups with non-bridging oxygen [27].

The absorption spectra of boron in the form of a boroxyl ring are given as BO_4 and BO_3 units in a glass structure. Around 800-1200 cm^{-1} region, corresponds to the stretching of tetrahedral BO_4^- units, while the transmission band around 1200-1800 cm^{-1} is associated with the B-O stretching of trigonal BO_3 units [28]. Within the range of 400-600 cm^{-1}, the vibration observed could be attributed to the Si–O–Si and O–Si–O bending modes of bridging oxygen in the glass structure [29]. Similarly, the vibration mode assigned to range 770-880 cm^{-1}, $940-860$ cm^{-1}, and 970-1095 cm^{-1} might also be due to the Si–O–Si symmetric stretch of bridging oxygen atoms between tetrahedra, Si–O–Si stretching of non-bridging oxygen atoms and Si–O–Si anti-symmetric stretch of bridging oxygen atoms between tetrahedral [29, 30] respec-

tively.

Origin 6.0 software was used to perform the deconvolution. In Figure 3, an example of the 0.03 ErDBST glass de-convoluted spectra was presented. The spectra show nine absorption bands assigned in the glass sample to various functional groups. The assignments for the bands are as well indicated in Figure 4. The bridging and non-bridging oxygens are formed simultaneously inside the glass structures. This is because of the different effects that erbium nanoparticles have on borate and tellurite glass. These changes structurally result in the modification of other properties of the glass. The band areas for all the concentrations are seen to vary independently with the concentration of dopant. These variations are due to the BO_4 to BO_3 conversion and TeO_4 to TeO_3 conversion and vice versa. Also, Figure 4 shows the variation of TO_3 and TO_4 in Er^{3+} NPs doped glass system. The TO_3 structural units increase in mole% from 0.01 to 0.03 of Er^{3+} NPs and then decrease in mole % at 0.04 and 0.05. The decrease in the band area with increasing dopant concentration indicates the non-bridging oxygen (NBO) formation within the glass structure. Whereas the decreasing trend of TeO_4 shows the formation of bridging oxygens decreases and the formation of non-bridging oxygens increase with the addition of dopants. Further increase in Er_2O_3 NPs will cause TeO_4 and BO_4 to TeO_3 and BO_3 conversion respectively. From Figure 5, it is observed that the BO_3 units are converted into BO_4 units with the increasing erbium oxide and silver oxide content, and further, the band area of the BO_4 band increases. Alternatively, both BO_3 and BO_4 decrease with the concentration increase in erbium nanoparticles, further increment in the dopant concentration tends to increase the BO_3 at 0.05 mole% of erbium oxide nanoparticles and silver oxide. The decreasing trend shows the formation of bridging oxygen decreases and the formation of more non-bridging oxygen atoms with the addition of dopants [31]. The vibrations of Er^{2+} and Er^{3+} are not observed in the system because; the amount of erbium used in the glass composition is relatively small, which completely takes part in the glass formation.
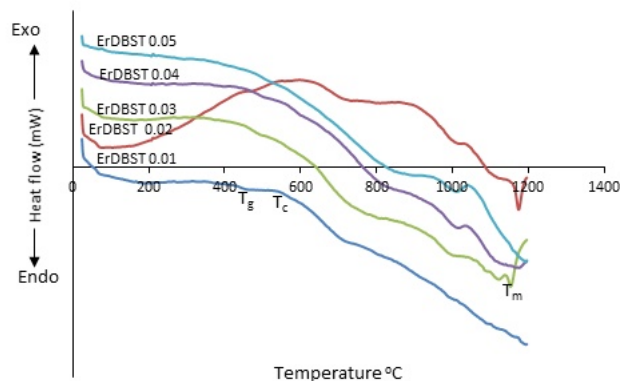

Figure 6. DSC profile of Er_2O_3 NPs doped bio-silica borotellurite glass system.
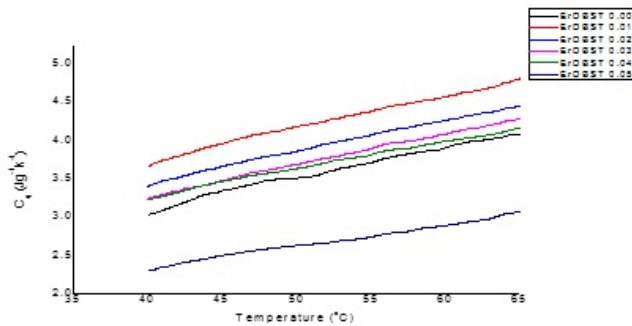
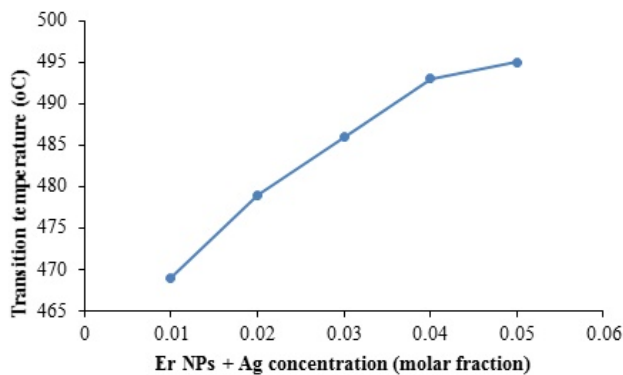**Figure 7.** Specific heat capacity of ErDBST glass system.

Figure 8. Variation of transition temperature with concentration in Er_2O_3 NPs in bio-silica borotellurite glasses.

3.2 Thermal analysis

Secondly, Figure 6 illustrates the erbium nanoparticles doped bio-silica borotellurite glass system based on the DSC curves. The detected values of the T_g, T_c, and T_m are listed in Table 2. The single and broad endothermic peak due to T_g shows the homogeneity in the two glass series. The exothermic peak, T_c, due to growth of the crystal, followed by another endothermic peak due to re-melting of the glass samples, T_m, was observed in all the erbium nanoparticles doped bio-silica borotellurite glasses at higher temperatures. The identification difficulty experienced in the glass transition peak T_g is due to the contraction of the glass [32]. These characteristics temperatures relied on the individual bond strength; therefore, the contraction does not affect the non-bridging oxygen present in the glass network.
The thermal stability is evaluated using the next equation

$$T_s = T_c - T_g \tag{1}$$

The higher the T_s value, give rise the delay in the nucleation process, the greater is the thermal stability, and the easier is the glass formation [33]. Moreover, Hruby parameter, H_r signifies the glass forming tendency and is given by

$$H_r = \frac{T_c - T_g}{T_m - T_c} \tag{2}$$

The difficulty in forming glasses with $H_r \leq 0.1$ requires a higher rate of cooling, while at a moderate quenching rate,

glasses with $H_r \geq 0.4$ can easily be formed [34].
Another parameter used to estimate the ability of glass-forming is the reduced glass transition temperature, T_{rg} obtained from the following:

$$T_{rg} = \frac{T_g}{T_m} \tag{3}$$

The glass transition temperature has a reduced value in the range $\frac{of1}{2} \leq T_{rg} \leq \frac{2}{3}$.
The criterion on thermodynamic fragility (F) gives information about the changes structurally that occur within the glass matrix and can be estimated by using Equation (4) depending on the parameters of the glass transition.

$$F = \frac{0.151 - \mu}{0.151 + \mu} \tag{4}$$

where $\mu = \frac{\Delta T_g}{T_g}$
However using Kissinger's method, the activation energy of the structural relaxation (E_g) is computed [35, 36] as shown in Equation (5)

$$\ln\left[\frac{T_g^2}{\beta}\right] = \frac{E_g}{R \times T_g} + constant \tag{5}$$

where β is the heating rate and R is the universal gas constant. The slope of the plot of $\ln(T_g^2/\beta)$ and $\ln(\beta)$ versus $(1000/T_g)$ respectively for the prepared glasses are used to compute the activation energies of the transition in the glass [37].
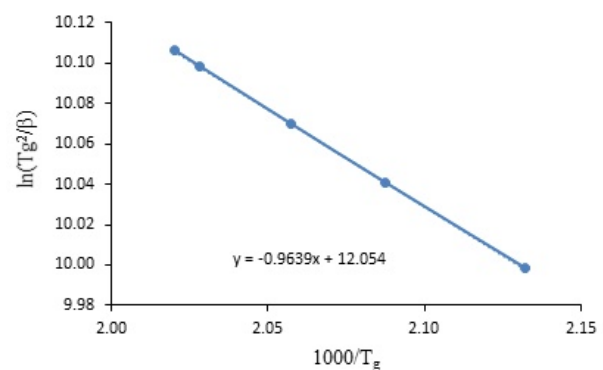The specific heat capacity of the glass sample is an important

Figure 9. Kissinger plot of Er_2O_3 NPs with Ag_2O doped bio-silica borotellurite glasses.

parameter to use to determine the stability and functionality of a material [38]. The following equation is used to compute the sample's specific heat capacity

$$C_q = \frac{1}{m}\frac{\delta Q}{\Delta T} = \frac{1}{m}\frac{(\delta Q/d\tau)}{(dT/d\tau)} \tag{6}$$

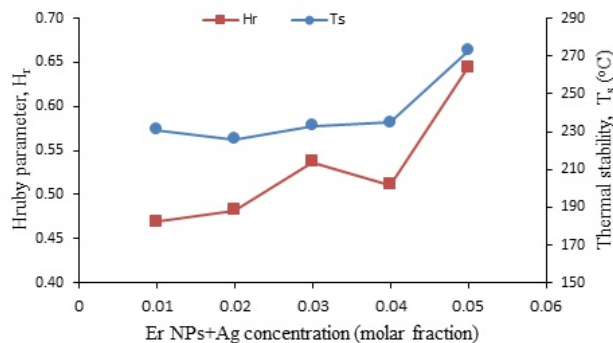where m is the mass of the sample, $\delta Q/d\tau$ is the heat

Figure 10. Variation of Hruby parameter and thermal stability with Er_2O_3 NPs concentration of bio-silica borotellurite glasses.
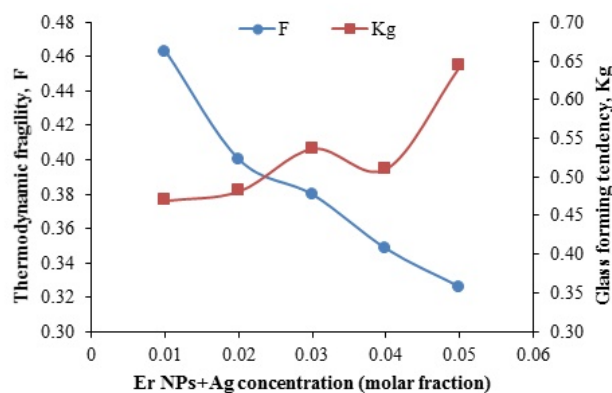

Figure 11. Variation of thermodynamic fragility and glass-forming tendency with Er_2O_3 NPs of bio-silica borotellurite glasses.

flux given by the DSC curve, m=mass of the sample, and $dT/d\tau = \beta$ is the sample's heating rate equal to 10 ^oC/min. The specific heat capacities for all prepared glass samples were found to increase with temperature, as given in Figure 7. The values are in the range of $2.2 - 4.5$ $Jg^{-1}K^{-1}$. The noticeable increase could be affected by the cooling rate of the glass [39]. Previously, both specific heat capacity and devitrification properties of tellurite glasses had been measured [40, 41].

The transition temperature, T_g, is plotted against the concentration of erbium nanoparticles with silver oxide doped glasses, as shown in Figure 8. It can be seen that the T_g of the glass series increases with an increase in dopant concentration in the figure. The increase in T_g with increment in Er^{3+} NPs/Ag^+ contents is connected to an increase in the glass network rigidity because of the increase of NBO (TeO_3). Additionally, the introduction of Ag_2O results in the Te-O bond length in TeO_3 units being smaller than in TeO_4 units, which provides the information that the bond strength of TeO_3 is higher than TeO_4 [33]. This result is supported by FTIR data. Moreover, in all the samples, the weak crystallization peak T_c is ascribed to the formation of heterogeneous nucleation sites facilitated

by the Ag_2O. The Kissinger method is the approach used to discuss the dependence which yields the activation energy, E_a of the glass series as given in Table 2. the activation energy according to the approach is obtained from the plot of $\ln(T_g/\beta)$ versus $(1000/T_g)$ as shown in Figure 9, and the evaluation of the activation energy, the slope of the straight line is used [37]. The value of the activation energy is constant with the increase in the concentration of erbium nanoparticles. This could be connected to the constant value of the heating rate used. The activation energy is 8010 J/mol for the studied glasses. The other two stability parameters studied are Hruby's factor (H_r) and thermal stability T_s that do not only represent the stability of the glass samples against devitrification but also indicate the glass-forming ability and thermal stability in the amorphous matrix [42].

Besides the above, Figure 10 represents the plot of the Hruby factor and thermal stability of $[\{[(TeO_2)_{0.8} (B_2O_3)_{0.2}]_{0.8} (SiO_2)_{0.2}\}_{0.99} (Ag_2O)_{0.01}]_{1-y} (Er_2O_3$ NPs$)_y$, glasses denoted by ErDBST, y=0.01,0.02,0.03,0.04 and 0.05 mole%. The two parameters show an increase in dopant concentration creating an increasing trend. The increase could be due to the absence or minimal growth of crystalline structure within or on the surface of the glass as the concentration of Er_2O_3 NPs increases. This result is also verified by the XRD analysis. Alternatively, the wider the thermal stability, T_s, is, the harder the glass is against the deformation of amorphous nature and conversion to crystallized glass-ceramics, ceramics, and crystals [11]. Interestingly, the values of T_s in the present glasses increased with the addition of the erbium nanoparticle oxides. Moreover, a decrease is observed at a 0.04 molar fraction of Er^{3+} NPs. This decrement might be attributed to the rupture Te-O-Te linkage by Er_2O_3 and Ag_2O. The obtained values of $T_{>}100$ ^oC and $H_r > 0.5$ indicated excellent stability and glass-forming ability of the bio-silica borotellurite glasses. The thermodynamic fragility, F, and glass-forming tendency, K_g illustrated in Figure 11, are important parameters that give information about the changes in the structure that exists in the glass matrix. The values of the thermodynamic fragility decrease from 0.463 to 0.326. The decrement seen in the values indicates that the fragility across the studied glasses is decreasing due to the increase in the connectivity of the glass, which is confirmed through the decrease in the molar volume. The increase in the glass forming tendency suggests the structural changes within the glass, which results in the conversion of TeO_4 to TeO_3 [43, 44].

4. Conclusion

$[\{[(TeO_2)_{0.8} (B_2O_3)_{0.2}]_{0.8} (SiO_2)_{0.2}\}_{0.99} (Ag_2O)_{0.01}]_{1-y}$ - $(Er_2O_3$ NPs$)_y$, where y=0.01,0.02,0.03,0.04 and 0.05 mole% had been achieved and investigated structurally and thermally. The erbium nanoparticles doped borosilicate tellurite glasses were fabricated using the melt quenching technique. XRF, XRD, FTIR, and DSC had been measured for every sample. The amorphous nature of the glasses was confirmed by the XRD results and it has been concluded that the impact of erbium

nanoparticles doped borosilicate tellurite glasses is as follows:
● Firstly, FTIR confirmed the glass samples' vibrational groups, and these vibrational modes give structural information about the glass samples, which includes the basic structural units such as TeO_4, TeO_3, BO_4, BO_3, Si-O-Si, and O-Si-O in the glass system. The quality achievement of 98.6% of silicate from rice husk was verified by XRF, which showed that silica, with 98.6%, is the rice husk ash's primary component.
● Secondly, the main thermal parameters T_g, T_c, T_s, and Hruby parameter, H_r had been increased from 469 to 495, 700 to 768, 231 to 273 ^{o}C, and 0.469 to 0.644. So, Er_2O_3 NPs and Ag_2O doped bio-silica borotellurite glass system thermal stability factor T_g is higher than 100 ^{o}C, which suggests that ErDBST glass is thermally stable glass and is suitable for a potential application in fiber drawing.

Conflict of interest statement:
The authors declare that they have no conflict of interest.

References

[1] N. N. Yusof, S. K. Ghoshal, and M. N. Azlan. *Journal of Alloys and Compounds*, **724**:1083, 2017.

[2] I. G. Geidam, K. A. Matori, M. K. Halimah, K. T. Chan, F. D. Muhammad, M. Ishak, S. A. Umar, and A. M. Hamza. *Optik*, **248**:12, 2021.

[3] U. S. Aliyu, H. M. Kamari, I. G. Geidam, I. O. Alade, A. M. Noorazlan, A. M. Hamza, and A. F. Ahmad. *Optical Materials*, **114**:110987, 2021.

[4] S. A. Umar, M. K. Halimah, G. G. Ibrahim, I. O. Alade, M. N. Azlan, R. El-Mallawany, A. M. Hamza, S. N. Nazrin, L .U. Grema, and M. S. Otto. *Ceramics International*, **47**:21668, 2021.

[5] A. M. Hamza, M. K. Halimah, F. D. Muhammad, and K. T. Chan. *Journal of Luminescence*, **207**:497, 2018.

[6] M. N. Azlan, M. K. Halimah, S. S. Hajer, A. B. Suraini, Y. Azlina, and S. A. Umar. *Chalcogenide Letters*, **16**:215, 2019.

[7] M. N. Azlan, M. K. Halimah, S. A. Umar, Y. Azlina, R. El-Mallawany, and G. Najmi. *Educatum Journal of Science, Mathematics and Technology*, **5**:47, 2018.

[8] F. D. Muhammad R. A. Tafida, M. K. Halimah, K.T. Chan, M.Y. Onimisi, A. Usman, A. M. Hamza, and S. A. Umar. *Materials Chemistry and Physics*, **246**:122801, 2020.

[9] S. H. Alazoumi, U. S. Aliyu S. A. Aziz, R. El-Mallawany, H. M. Kamari, M. H. M. M. Zaid, K. A. Matori, and A. Ushah. *Results in Physics*, **9**:1371, 2018.

[10] S. A. Umar, M. K. Halimah, M. N. Azlan, L. U. Grema, G. G. Ibrahim, A. F. Ahmad, A. M. Hamza, and M. M. Dihom. *SN Applied Sciences*, **291**:1, 2020.

[11] Z. A. Said Mahraz, M. R. Sahar, and S. K. Ghoshal. *Journal of Molecular Structure*, **1072**:238, 2014.

[12] A. Kaur, A. Khanna, and L. I. Aleksandrov. *Journal of Non-Crystalline Solids*, **476**:67, 2017.

[13] S. A. Umar, M. K. Halimah, K. T. Chan, A. A. Amirah, M. N. Azlan, L. U. Grema, A. M. Hamza, and G. G. Ibrahim. *Journal of Materials Science: Materials in Electronics*, **30**:18606, 2019.

[14] M. K. Halimah, S. A. Umar, K. T. Chan, A. A. Latif, M. N. Azlan, A. I. Abubakar, and A.M. Hamza. *Materials Chemistry and Physics*, **238**:121891, 2019.

[15] Y. Azlina, M. N. Azlan, S. S. Hajer, M. K. Halimah, A. B. Suriani, S. A. Umar, R. Hisam, M. H. M. Zaid, S. M. Iskandar, B. K. Kenzhaliyev, A. V. Nitsenko, N. N. Yusof, and I. Boukhris. *Optical Materials*, **117**:111138, 2021.

[16] A. M. Hamza, M. K. Halimah, F. D. Muhammad, K. T. Chan, A. Usman, M. F. Faznny, I. Zaitizila, and R. A. Tafida. *Results in Physics*, **14**:102457, 2019.

[17] G. Lakshminarayana, K. M. Kaky, S. O. Baki, A. Lira, P. Nayar, I. V. Kityk, and M. A. Mahdi. *Journal of Alloys and Compounds*, **690**:799, 2017.

[18] R. El-Mallawany. *Journal of applied physics*, **73**:4878, 1993.

[19] R. N. Hampton, W. Hong, G. Saunders, and R. A. El-Mallawany. *Physics and Chemistry of Glasses*, **29**:100, 1988.

[20] A. El-Adawy and R. El-Mallawany. *Journal of materials science letters*, **15**:2065, 1996.

[21] R. El-Mallawany, M. Sidkey, A. Khafagy, and H. Afifi. *Materials chemistry and physics*, **37**:295, 1994.

[22] Q. Liu, Y. Tian, W. Tang, X. Jing, J. Zhang, and S. Xu. *Nanophotonics*, **7**:913, 2018.

[23] T. Lee, R. Othman, and F. Y. Yeoh. *Biomass and Bioenergy*, **59**:380, 2013.

[24] S. T. Glasses. *Journal of Pure and Applied Sciences*, **29**:32, 2017.

[25] A. Awang, S. K. Ghoshal, M. R. Sahar, M. Reza Dousti, R. J. Amjad, and F. Nawaz. *Current Applied Physics*, **13**:1813, 2013.

[26] S. A. Umar, M. K. Halimah, K. T. Chan, and A. A. Latif. *Journal of Non-Crystalline Solids*, **472**:31, 2017.

[27] B. Eraiah. *Bulletin of Materials Science*, **33**:391, 2010.

[28] L. Bolundut, E. Culea, G. Borodi, R. Stefan, C. Munteanu, and P. Pascuta. *Ceramics International*, **41**:2931, 2015.

[29] S. A. Umar, M. K. Halimah, A. M. Hamza, and A. A. Abdulbaset. *Journal of Science and Mathematics Letters*, **6**:32, 2018.